Materials Transactions, Vol. 45, No. 7 (2004) pp. 2078 to 2082
Special Issue on Grain Boundaries, Interfaces, Defects and Localized Quantum Structures in Ceramics

Improvement of High-temperature Creep Resistance in Polycrystalline Al_2O_3 by Cations Co-doping

Shuichi Yasuda*, Hidehiro Yoshida, Takahisa Yamamoto and Taketo Sakuma

Department of Advanced Materials Science, Graduate School of Frontier Sciences, The University of Tokyo, Tokyo 113-8656, Japan

High-temperature creep resistance in cations co-doped polycrystalline Al_2O_3 was examined by uniaxial compression creep test at 1250°C. The dopant oxides used in this study were 0.1 mol% of $YO_{1.5}$, ZrO_2, SrO, MgO and TiO_2. The creep rate in Al_2O_3 was significantly changed by cations co-doping. For instance, Zr/Y co-doping suppressed the creep rate in Al_2O_3 by a factor of about 400. A high-resolution transmission electron microscopy (HREM) and nano-probe energy dispersive X-ray spectroscopy (EDS) analysis revealed that Y and Zr cations segregate along grain boundaries. The grain boundary diffusion in Al_2O_3 was supposed to be retarded by the segregation of Y and Zr cations. A first-principle molecular orbital calculation was made for cations co-doped Al_2O_3 and cation singly doped Al_2O_3 model cluster. The creep rate was correlated with the value of net charge in oxygen anion. The net charge of oxygen anion was one of the most important factors to determine the creep resistance in Al_2O_3.

(Received January 30, 2004; Accepted April 6, 2004)

Keywords: *co-doped alumina, creep, ionicity, grain boundary, molecular orbital calculation*

1. Introduction

High-temperature creep deformation or plastic flow behavior in fine-grained polycrystalline Al_2O_3 is sensitively affected by small amount of dopant cation, which tends to segregate along grain boundaries.[1–3] For example, the high-temperature creep resistance in Al_2O_3 with the grain size of about 1 μm is markedly improved by ZrO_2, $YO_{1.5}$ or $LuO_{1.5}$ doping even in the dopant level of 0.1 mol%.[1–3] A first-principle molecular orbital calculation revealed that the creep rate in cation singly doped Al_2O_3 was found to correlate with ionic bond strength between aluminum cation and oxygen anion.[4]

The creep resistance has also been examined in cations co-doped Al_2O_3.[5–7] For instance, it has been reported that Nd/Zr co-doped Al_2O_3 exhibited superior creep resistance than Nd or Zr singly doped Al_2O_3.[7] However, the co-doping effect has not been systematically examined, and the origin of the effect of cations co-doping on the creep resistance in Al_2O_3 has not been clarified yet. The purpose of this paper is to examine the effect of cations co-doping on the high-temperature creep resistance in Al_2O_3. In this study, divalent cation (Mg^{2+}, Sr^{2+}), trivalent cation (Y^{3+}) and tetravalent cation (Ti^{4+}, Zr^{4+}) were used as dopant cations to examine the creep resistance in cations of various valencies doped Al_2O_3. Cation singly doped Al_2O_3 exhibits different creep resistance for each dopant cation.[4] We can compare the effect of caions co-doping on the creep resistance with that of cation singly doping. The origin of the effect of cations co-doping will be discussed from the viewpoint of chemical bonding strength at the grain boundaries.

2. Experimental Procedure

The materials used in this study were undoped, high-purity Al_2O_3 and two cations co-doped Al_2O_3. The dopant oxides used in this study were TiO_2, MgO, SrO, ZrO_2 and $YO_{1.5}$. The amount of dopant cation was controlled to be 0.1 mol% for each dopant oxide, *i.e.*, the total amount of dopant cations in cations co-doped Al_2O_3 is 0.2 mol%. The amount of dopant cation in cation singly doped Al_2O_3 is 0.1 mol%. High-purity Al_2O_3 powders with 99.99% purity (TM-DAR, Taimei Chemicals, Japan), yttrium acetate, strontium acetate and magnesium acetate (99.9%, Rare Metallic, Tokyo, Japan), titanium oxide powder (Sumitomo Osaka Cement, Japan) and zirconium oxide powder (0Y-TZP; Tosoh, Japan) were used for starting materials. Detailed fabrication procedure is described elsewhere.[4] The green compacts were sintered at temperature in a range of 1300°C-1550°C for 2 h in air to obtain an average grain size of about 1 μm. The grain size was measured by a linear intercept method using scanning electron microscope (SEM) photographs. The composition and the sintering temperature in the present materials were shown in Table 1.

High-temperature creep experiments were carried out under uniaxial compression in air at a constant load using a lever-arm testing machine with a resistance-heated furnace (HCT-1000, Toshin Industry, Tokyo, Japan). The applied stress and temperature were 50 MPa and 1250°C, respectively. The testing temperature was measured by Pt-PtRh thermocouple attached to each specimen and kept to within ±1°C. The size of the specimens was $5 \times 5\,mm^2$ in cross-section and 7 mm in height for compression tests.

High-resolution electron microscopy (HREM) was performed to observe the grain boundary structure using a JEOL-2010 field-emission-type electron microscope. Chemical analysis was carried out by an X-ray energy dispersive spectrometer (EDS) attached to the microscope with a probe size of less than 1 nm. From the Mulliken's population analysis, net charge (NC) for each ion, which corresponds to effective ionic valency, can be obtained. In this study, NC of six oxygen anions was estimated in order to compare the change of chemical bonding state in cations co-doped Al_2O_3 and cation singly doped Al_2O_3. These six oxygen anions were the first-neighbor of the aluminum cation that was in the center of cluster shown in Fig. 1.

In order to estimate chemical bonding state in pure and cation-doped Al_2O_3, a first-principle molecular orbital

*Corresponding author, E-mail: yasuda@ceramic.mm.t.u-tokyo.ac.jp

Table 1 The composition, sintering temperature and number of cations and vacancies introduced in model clusters used for the molecular orbital calculation in the present materials.

Composition	Name	Sintering temperature (°C)	Dopant in molecular orbital calculatiion
0.1 mol%TiO_2-0.1 mol%MgO doped Al_2O_3	Ti/Mg	1310	$Ti^{4+} \times 3$, $Mg^{2+} \times 3$
0.1 mol%TiO_2-0.1 mol%$YO_{1.5}$ doped Al_2O_3	Ti/Y	1380	$Ti^{4+} \times 3$, $Y^{3+} \times 3$, $V(Al^{3+}) \times 1$
0.1 mol%MgO-0.1 mol%SrO doped Al_2O_3	Mg/Sr	1385	$Mg^{2+} \times 3$, $Sr^{2+} \times 3$, $V(O^{2-}) \times 3$
0.1 mol%MgO-0.1 mol%ZrO_2 doped Al_2O_3	Mg/Zr	1410	$Mg^{2+} \times 3$, $Zr^{4+} \times 3$
0.1 mol%SrO-0.1 mol%$YO_{1.5}$ doped Al_2O_3	Sr/Y	1420	$Sr^{2+} \times 2$, $Y^{3+} \times 3$, $V(O^{2-}) \times 1$
0.1 mol%ZrO_2-0.1 mol%$YO_{1.5}$ doped Al_2O_3	Zr/Y	1430	$Y^{3+} \times 3$, $Zr^{4+} \times 3$, $V(Al^{3+}) \times 1$
0.1 mol%TiO_2 doped Al_2O_3	Ti	1285	$Ti^{4+} \times 6$, $V(Al^{3+}) \times 2$
0.1 mol%MgO doped Al_2O_3	Mg	1300	$Mg^{2+} \times 6$, $V(O^{2-}) \times 3$
0.1 mol%SrO doped Al_2O_3	Sr	1350	$Sr^{2+} \times 6$, $V(O^{2-}) \times 3$
0.1 mol%ZrO_2 doped Al_2O_3	Zr	1400	$Zr^{4+} \times 6$, $V(Al^{3+}) \times 2$
0.1 mol%$YO_{1.5}$ doped Al_2O_3	Y	1400	$Y^{3+} \times 6$

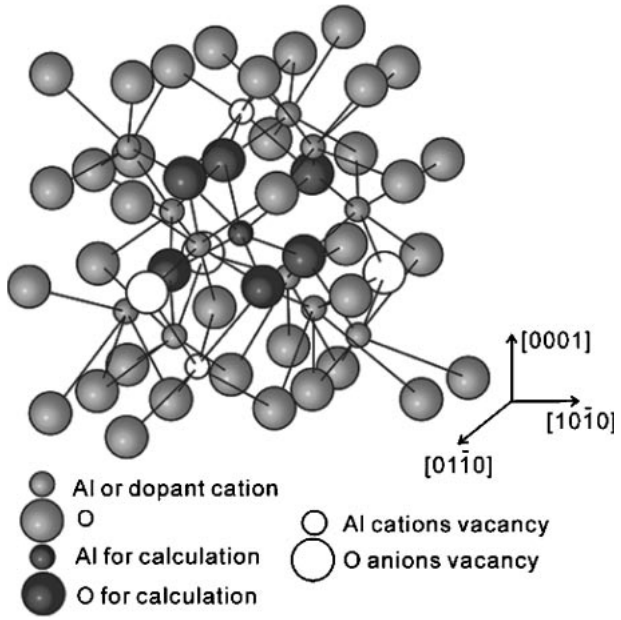

Fig. 1 A schematic illustration of atomic structure of cluster model $[Al_{14}O_{45}]^{48-}$ used for a first-principle molecular orbital calculation.

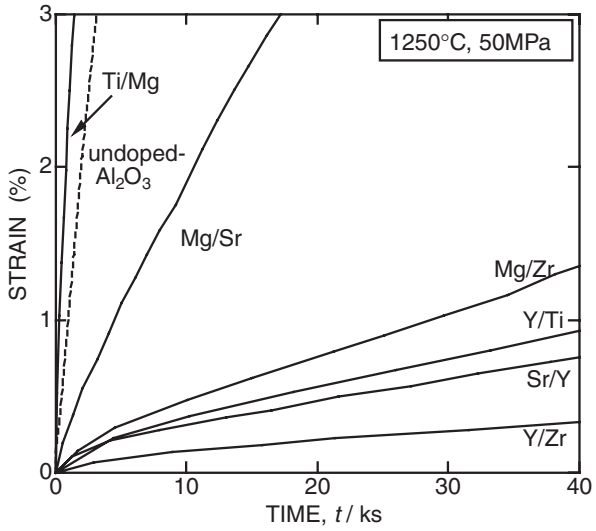

Fig. 2 Creep curves in undoped, high-purity Al_2O_3, and 0.1 mol% of TiO_2, MgO, SrO, ZrO_2 or $YO_{1.5}$ co-doped Al_2O_3 under an applied stress of 50 MPa at 1250°C.

calculation was made using DV-Xα method.[8] Figure 1 shows a model cluster of $[Al_{14}O_{45}]^{48-}$ for undoped-Al_2O_3 used in this study. In the model cluster, oxygen anions formed a close-packed structure and all aluminum cations took the octahedral coordination. The model cluster is for pure Al_2O_3 corundum structure, not for grain boundaries in Al_2O_3. However, it is impossible at the present stage to construct a general grain boundary structure for the molecular orbital calculation. In this study, the ionic bonding state in Al_2O_3 was approximately estimated using the model clusters without atomic configuration of the grain boundary in Al_2O_3. The white circles in Fig. 1 indicate O^{2-} anion's vacancies introduced in divalent cation doped Al_2O_3 and Al^{3+} cation's vacancies introduced in tetravalent cation doped Al_2O_3 to maintain electronic neutrality. The dopant cations and accompanying vacancies in the cation-doped Al_2O_3 model clusters are listed in Table 1.

3. Results and Discussion

Figure 2 shows the creep curves in the present materials under an applied stress of 50 MPa at 1250°C. The creep behavior in Al_2O_3 is considerably changed by cations co-doping, though the amount of dopant cations is quite small. The creep deformation in Al_2O_3 is suppressed by Ti/Y, Mg/Sr, Mg/Zr, Zr/Y or Sr/Y co-doping, and in particular, Zr/Y co-doping improves the high-temperature creep resistance remarkably. On the other hand, the creep deformation in Ti/Mg co-doped Al_2O_3 is accelerated in comparison with undoped Al_2O_3.

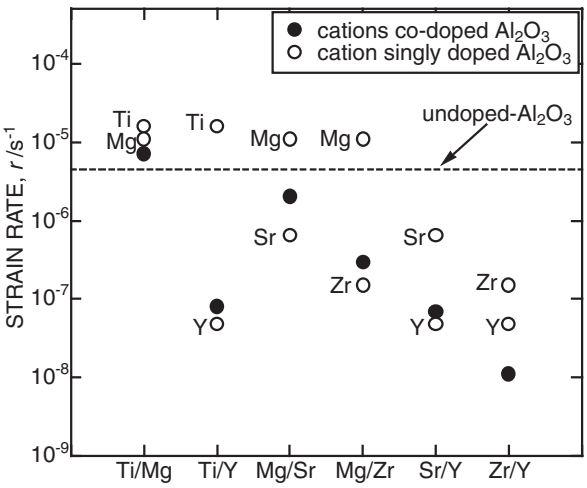

Fig. 3 Creep rates in undoped, high-purity Al_2O_3, and 0.1 mol% of TiO_2, MgO, SrO, ZrO_2 or $YO_{1.5}$ co-doped or singly doped Al_2O_3 under an applied stress of 50 MPa at 1250°C.

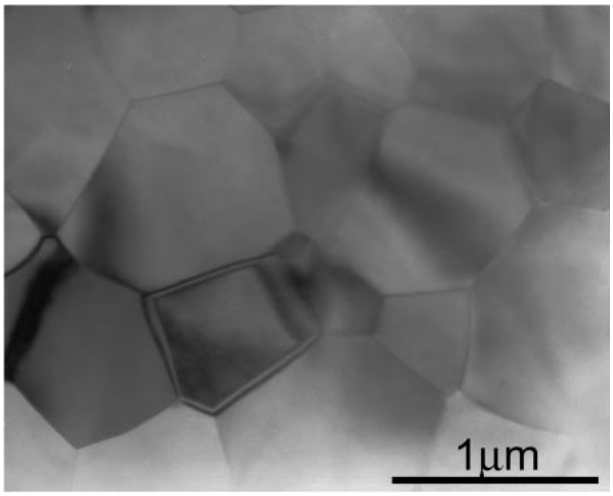

Fig. 4 A bright field image of 1% deformed Al_2O_3 co-doped with 0.1 mol% $YO_{1.5}$ and 0.1 mol% ZrO_2.

Figure 3 shows the steady-state creep rate in the present materials at 1250°C under an applied stress of 50 MPa. In this study, the steady-state creep region is defined where the change of strain rate with time is in the level of $\pm 1 \times 10^{-8}\,s^{-1}$. The creep rate of Ti/Y, Mg/Sr, Mg/Zr, and Sr/Y co-doped Al_2O_3 is in a range of the creep rates in each cation singly doped Al_2O_3. On the other hand, the creep rate of Ti/Mg or Zr/Y co-doped Al_2O_3 is smaller than that in each cation singly doped Al_2O_3. In particular, the creep rate of Zr/Y co-doped Al_2O_3 is much lower than that in undoped Al_2O_3 by a factor of about 400. The present result indicates that the creep rate in cations co-doped Al_2O_3 can not be expected from that in cation singly doped Al_2O_3.

The total amount of dopant cations in cations co-doped Al_2O_3 are larger than that in cation singly doped Al_2O_3. However, in the previous study, the creep resistance in 0.1 mass% ZrO_2 doped Al_2O_3 was found to be not so different from that in 10 wt% ZrO_2 doped Al_2O_3.[1)] This fact indicates that the difference in the amount of dopant cations over about 0.1 mol% does not strongly affect the creep resistance in Al_2O_3. Therefore, the effect of the difference in the amount of dopant cations on the creep resistance was probably negligible in the present materials.

Figure 4 shows a bright field image of Zr/Y co-doped Al_2O_3, which was deformed to be 1%. The average grain size is about 1 μm. The grain growth during creep deformation was negligible in the present material at the temperature examined. There is no intragranular dislocation in the crept sample. This fact indicates that the creep deformation takes place by diffusional processes.

Figure 5(a) shows a HREM image of a grain boundary in Zr/Y co-doped Al_2O_3. No amorphous phase or precipitation of second phase particles was observed along the grain boundary. Figures 5(b) and (c) demonstrate EDS spectra taken from the grain interior and the grain boundary, respectively. The analyzed points are indicated by circles in Fig. 5(a). The peak indicating Cu is the signal from the sample holder. The EDS analysis revealed that Y and Zr cations presented along the grain boundary but not in the grain interior. This data indicates that Y and Zr cations segregate along the grain boundary.

In polycrystalline Al_2O_3, high-temperature creep deformation often occurs by a diffusional process.[9–16)] The predominant deformation mechanism in Al_2O_3 with the grain size of less than about 10 μm is grain boundary diffusion creep at temperatures of 1100-1400°C and under a stress of less than 100 MPa,[9–12)] and the grain boundary sliding contributes dominantly to the creep deformation when the grain size is less than about 2 μm.[13–16)] It has been reported that the creep deformation in fine-grained Al_2O_3 with the average grain size of about 1 μm takes place by grain boundary sliding accommodated by grain boundary diffusion.[17–20)] Since the dopant cations segregate along the grain boundaries, and since the creep deformation is rate-controlled by the grain boundary diffusion, the improvement of creep resistance in cations co-doped Al_2O_3 is likely to result from the suppression of the grain boundary diffusion due to the segregation of dopant cations.

Figure 6 shows the steady-state creep rate against ionic radius of dopant cations.[21)] Ionic radius of dopant cations in cations co-doped Al_2O_3 is defined as an average radius of the two cations. As seen in this figure, the creep rate cannot be explained solely from the ionic radius. For example, the ionic radius in Zr/Y co-doped Al_2O_3, which exhibits the lowest creep rate in the present materials, has an intermediate value in comparison with ionic radiuses in other cation-doped Al_2O_3. On the other hand, Sr^{2+} cation, which has largest ionic radius, retards the creep rate of Al_2O_3, but the strain rate is rather close to that in undoped Al_2O_3.

In cation singly doped Al_2O_3, a change in chemical bonding strength is supposed to be one of the most important factors to determine the creep rate.[4)] The change in ionicity was examined in cation-doped Al_2O_3, and we found good correlation between the creep rate and the value of NC in oxygen anion. Figure 7 shows a plot of the creep rate in the present materials against the value of NC in oxygen anion. In this study, the largest value of NC in six oxygen anions was used as the value of NC in O. The NC in O correlated with the creep rate both in cation singly doped Al_2O_3 and cations co-

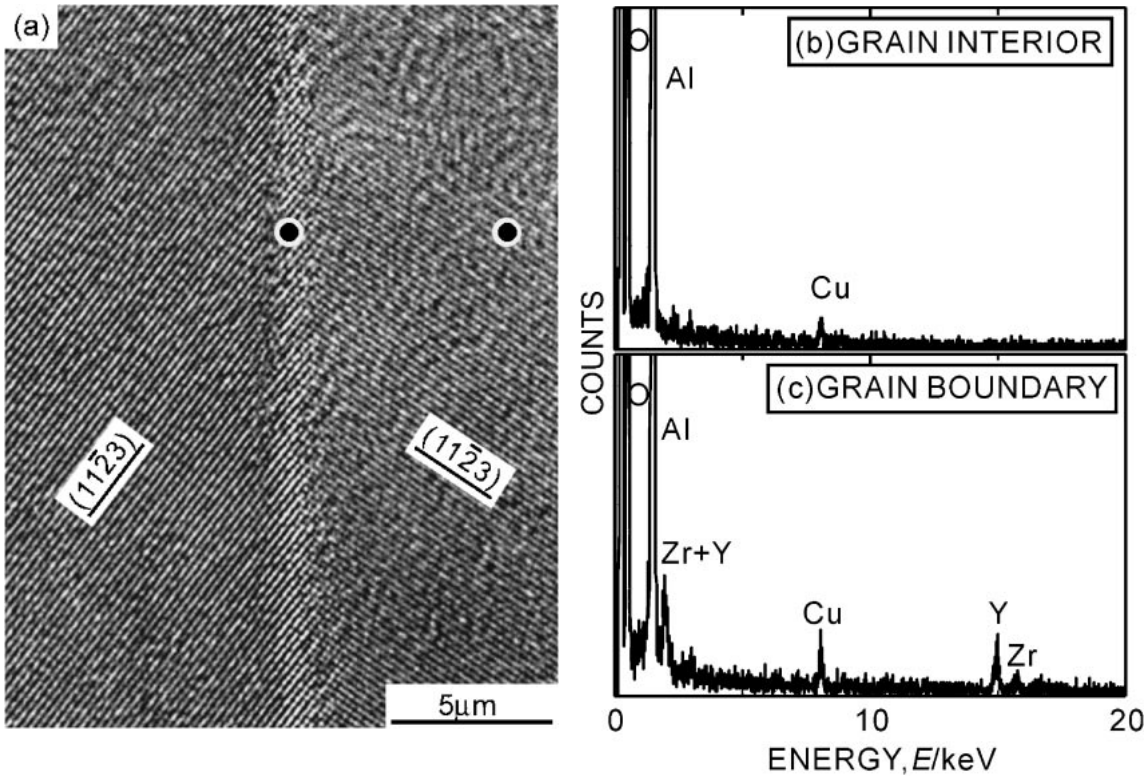

Fig. 5 (a) A high-resolution electron micrograph for a grain boundary in 1% deformed Al_2O_3 co-doped with 0.1 mol% $YO_{1.5}$ and 0.1 mol% ZrO_2. EDS spectra are also demonstrated (b) for the grain interior and (c) for the grain boundary using a prove size of about 1 nm. The analyzed points are indicated by circles in Fig. 5(a).

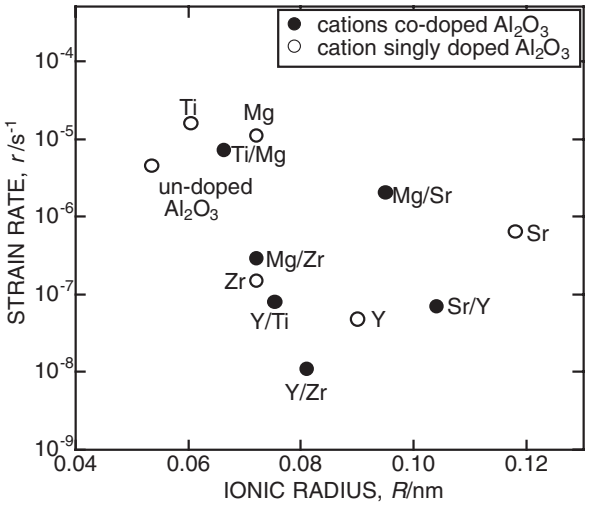

Fig. 6 The steady-state creep rate under an applied stress of 50 MPa and 1250°C in the present materials against the ionic radius of the dopant cation. The ionic radius in co-doped Al_2O_3 defined as average radius of two dopant cations. The ionic radius is six-folded coordination.[21)]

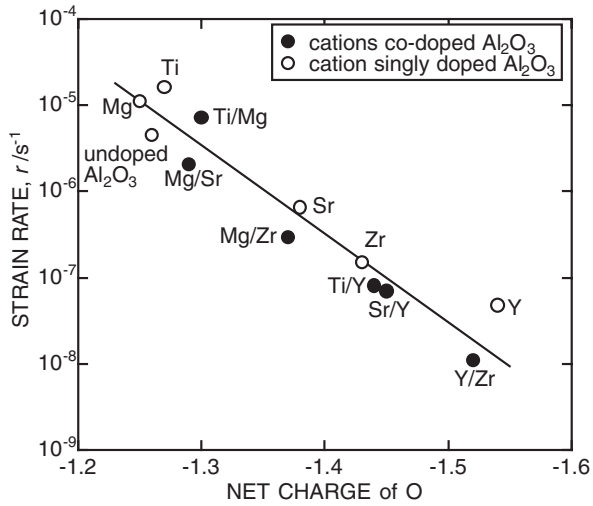

Fig. 7 The steady-state creep rate under an applied stress of 50 MPa and 1250°C in the present materials against the net charge of oxygen anion.

doped Al_2O_3. The increase of NC in O can be regarded as the increase of ionic charge in oxygen anion. The ionicity in oxygen anion probably corresponds to the Coulomb's attractive force between oxygen anion and cations that were the nearest neighbor of the oxygen anion, because the Coulomb's attractive force is proportional to the ionic charge of anion and cation. The increase in the Coulomb's attractive force may suppress the grain boundary diffusion of oxygen anion. This result indicates that the change of chemical bonding state in oxygen anion must affect the grain boundary diffusion in cations co-doped Al_2O_3.

In the previous studies, it has been reported that the creep deformation in fine-grained Al_2O_3 with the average grain size of less than 10 μm is rate-controlled by the grain boundary diffusion of aluminum cation.[1,3,22)] However, a recent study reported that the grain boundary diffusion of oxygen anion is the rate-controlling mechanism for the creep deformation in Al_2O_3.[23)] The present calculation indicates that the rate-

controlling species in creep deformation in Al_2O_3 may be oxygen anion. This result is consistent with the previous study.[23] This fact indicates that the ionic bonding state, particularly the ionic charge of oxygen anion, is an important factor to determine the creep resistance and the grain boundary diffusion in Al_2O_3. Further investigation on the matter transport phenomena and chemical bonding state in the vicinity of the grain boundaries will provide more quantitative relationship between the diffusivity and the ionic bond strength.

4. Conclusion

High temperature creep resistance was examined in 0.2 mol% cations co-doped Al_2O_3. The creep rate in Al_2O_3 is sensitively influenced by cations co-doping, but the co-doping effect cannot be explained from the effect of cation singly doping. The creep rate in Y/Zr co-doped Al_2O_3 is much lower than that in undoped Al_2O_3 by a factor of about 400. HREM observation and nano-prove EDS analysis revealed that Y and Zr cations segregate along the grain boundary. Since the creep deformation in undoped Al_2O_3 takes place by grain boundary sliding accommodated by grain boundary diffusion, the grain boundary diffusion in Al_2O_3 is probably retarded by the segregation of Y and Zr cations. A first-principle molecular orbital calculation based on $[Al_{14}O_{45}]^{48-}$ model cluster revealed that the value of NC in O correlates with the creep rate in cations co-doped Al_2O_3. The creep resistance in cations doped Al_2O_3 is likely to be determined by ionicity of oxygen anion at the grain boundaries with dopant cations segregation.

Acknowledgements

The authors wish to express their gratitude to the Ministry of Education, Science, Culture, Sports, Science and Technology Japan for their financial aid by a Grant-in-Aid for Scientific Research and Grant-in-Aid for Encouragement of Young Scientists. The authors also wish to express their thanks to Nippon Sheet Glass Foundation for Materials Science and Engineering.

REFERENCES

1) H. Yoshida, K. Okada, Y. Ikuhara and T. Sakuma: Phil. Mag. Lett. **76** (1997) 9–14.
2) J. Cho, M. P. Harmer, H. M. Chan, J. M. Rickman and A. M. Thompson: J. Am. Ceram. Soc. **80** (1997) 1013–1017.
3) H. Yoshida, Y. Ikuhara and T. Sakuma: J. Mater. Res. **13** (1998) 2597–2601.
4) H. Yoshida, Y. Ikuhara and T. Sakuma: Acta Mater. **50** (2002) 2955–2966.
5) S. Latigue, C. Carry and L. Priester: J. Phys. Cl. **51** (1990) 985–990.
6) A. G. Robertson, D. S. Wilkinson and C. H. Caceres: J. Am. Ceram. Soc. **74** (1991) 915–921.
7) Y. Z. Li, C. Wang, H. M. Chan, J. M. Rickman and M. P. Harmer: J. Am. Ceram. Soc. **82** (1999) 1497–1504.
8) H. Adachi, M. Tsukada and C. Satoko: J. Phys. Soc. Jpn. **45** (1978) 875–883.
9) A. E. Paladino and R. L. Coble: J. Am. Ceram. Soc. **46** (1963) 133–136.
10) A. H. Heuer, R. M. Cannon, N. J. Tighe, J. J. Burke, N. L. Reed, V. Weiss and editors: *Ultrafine-grain ceramics. Syracuse, NY*, (Syracuse University Press, 1970) pp. 339–65.
11) T. G. Langdon and F. A. Mohamed: J. Mater. Sci. **13** (1973) 473–482.
12) A. H. Heuer, N. J. Tighe and R. M. Cannon: J. Am. Ceram. Soc. **63** (1980) 53–58.
13) H. J. Frost and M. F. Ashby: *Deformation-mechanism maps. Oxford*, (Pergamon, 1982).
14) A. H. Chokshi and J. R. Porter: J. Mater. Sci. **21** (1986) 705–710.
15) A. H. Chokshi and T. G. Langdon: Mater. Sci. Tech. **25** (1991) 577–584.
16) A. H. Chokshi. J. Mater. Sci. **25** (1990) 3221–3228.
17) R. C. Gifkins: Metall. Trans. A **7** (1976) 1225–1232.
18) T. G. Langdon: Philos. Mag. **22** (1970) 689–700.
19) A. K. Mukherjee: Mater. Sci. Eng. **8** (1971) 83–89.
20) A. Arieli and A. K. Mukherjee. Mater. Sci. Eng. **45** (1980) 61–70.
21) R. D. Shannon: Acta Cryst. **A32** (1976) 751–767.
22) R. M. Cannon, W. H. Rhodes and A. H. Heuer: J. Am. Ceram. Soc. **63** (1980) 46–53.
23) O. A. Ruano, J. Wadsworth and O. D. Sherby: Acta Mater. **51** (2003) 3617–3634.